Journal of Alloys and Compounds 500 (2010) 167–174

Contents lists available at ScienceDirect

Journal of Alloys and Compounds

journal homepage: www.elsevier.com/locate/jallcom

Effects of Ce and Zn additions on the microstructure and mechanical properties of Sn–3Ag–0.5Cu solder joints

Hsiu-Jen Lin[a,b], Tung-Han Chuang[a,*]

[a] Institute of Materials Science and Engineering, National Taiwan University, No. 1, Sec. 4, Roosevelt Road, Taipei 106, Taiwan
[b] Industrial Technology Research Institute, Mechanical and Systems Research Laboratories, Hsinchu 310, Taiwan

ARTICLE INFO

Article history:
Received 14 December 2009
Received in revised form 24 March 2010
Accepted 31 March 2010
Available online 8 April 2010

Keywords:
Sn–3Ag–0.5Cu–0.5Ce–0.2Zn solder
BGA packages
Au/Ni/Cu pads
Intermetallic compounds
Mechanical properties

ABSTRACT

It has been reported that the rapid growth of tin whiskers occurring on the surface of rare earth containing solders can be prevented by the addition of 0.5 wt.% Zn into a Sn–3Ag–0.5Cu–0.5Ce alloy. The present study shows that the tensile strength of Sn–3Ag–0.5Cu–0.5Ce alloy alloyed with Zn increases significantly in comparison to the Zn-free Sn–3Ag–0.5Cu and Sn–3Ag–0.5Cu–0.5Ce solder. Moreover, the growth of intermetallic compounds at the solder/pad interfaces during the thermal aging at 100 °C and 150 °C was inhibited by the Zn addition. Nevertheless, the excess of Zn addition to 0.5 wt.% causes poor junction in the Sn–3Ag–0.5Cu–0.5Ce packages. An optimized addition amount of Zn in Sn–3Ag–0.5Cu–0.5Ce solders is 0.2 wt.% for both inhibiting the growth of tin whiskers and strengthening the solder joints, although its ductility is still lower than that of the original Sn–3Ag–0.5Cu.

1. Introduction

Owing to the advantages of long thermal fatigue life and improved creep resistance, the eutectic Sn–Ag–Cu system has been considered as one of the most promising alloys for the replacement of traditional Sn–37Pb solder [1]. For further improvement of its performance, many efforts have been made through the additions of fourth elements. Recently, rare earth (RE) elements have also been employed for the alloying of lead-free solder alloys, through which many beneficial effects have been reported [2–5]. For the Sn–0.5Cu–0.05Ni solders, the interface energy was reduced and the resistance of grain growth increased due to the addition of Ce [6]. Shiue and Chuang found that the growth of interfacial intermetallics layers in Sn–58Bi–0.5La packages with Au/Ni/Cu pads was much smaller than those in the undoped Sn–58Bi [7]. Xiao et al. found that the creep-fatigue rupture lifetime of Sn–3.8Ag–0.7Cu increased with small additions of mixed metal (Ce, La) [8]. Moreover, the mechanical strength, wettability, and creep rupture life of Sn–3.8Ag–0.7Cu solder alloy were improved by doping with 0.05–0.25 wt.% Er [9]. Dudek et al. reported that the strain to failure of Sn–3.9Ag–0.7Cu solder increased nearly 46% and 150% after alloying with 0.5 Ce and 0.5 wt.% La, respectively [10,11]. However, an amazingly rapid growth of long fiber shaped tin whiskers has been observed on the surface of rare-earth-doped Sn–3Ag–0.5Cu–0.5Ce solder joints of ball grid array (BGA) packages after air exposure at room temperature for several days [12]. Further study showed that hillock-type whiskers occurred on this solder during storage in a 150 °C air furnace for several minutes [13]. Since the appearance of tin whiskers in solder joints can cause electronic devices to short circuit, the alloying of Sn–Ag–Cu solders with rare earth elements could be risky for industrial applications. Fortunately, Chuang and Lin observed that the rapid growth of tin whiskers was prevented in a Sn–9Zn–0.5Ce solder, which is attributed to the refining of its $(Ce_{0.9}Zn_{0.1})Sn_3$ intermetallic clusters [14]. A similar result can be obtained in Sn–9Zn–0.5La solder joints [15]. Such an inhibition effect on the whisker growth has also been adopted in a Sn–3Ag–0.5Cu–0.5Ce alloy doped with 0.5 wt.% Zn [16]. Although the addition of Zn into Sn–3Ag–0.5Cu–0.5Ce solder can effectively prevent the rapid growth of tin whiskers, its effects on the mechanical properties and microstructure of this alloy should be evaluated. Wang et al. has reported that a small addition of Zn into Sn–0.7Cu solder can significantly inhibit the growth of interfacial Cu_6Sn_5 intermetallic compounds during solidification process [17]. Kang et al. also found that the minor Zn alloying into Sn–Ag–Cu solder can reduce undercooling during solidification and thus prevent the formation of large Ag_3Sn plates [18]. Further study by Wang et al. showed that during solid-state isothermal aging treatments of the Sn–3Ag–0.5Cu solder doped with 0.2 wt.% Zn, the intermetallic compounds at the interfaces between this solder alloy and Cu substrate were remarkably reduced, which were more prominent at higher aging temperature [19]. According to their thermodynamic analyses, the depressing effect of intermetal-

* Corresponding author.
E-mail address: tunghan@ntu.edu.tw (T.-H. Chuang).

0925-8388/$ – see front matter © 2010 Elsevier B.V. All rights reserved.
doi:10.1016/j.jallcom.2010.03.233

lic compounds was attributed to the lower activation energy for the intermetallics growth at Sn–3Ag–0.5Cu–0.2Zn/Cu interfaces than that at the undoped Sn–3Ag–0.5Cu/Cu and the decrease of diffusion coefficient for the Zn containing Sn–Ag–Cu solder/Cu system. On the other hand, the addition of rare earth elements into Sn–Zn alloys has been reported to be beneficial in many aspects. Wu et al. indicated that the tensile strength and yield strength of Sn–9Zn were improved by alloying with 0.05 and 0.5 wt.% (Ce, La) mixed metal [20]. The beneficial effects on the mechanical properties were connected to the refinement of the β-Sn grains in rare-earth-doped Sn–9Zn solder. Further study by Wu et al. revealed that the wettability of Sn–9Zn solder containing 0.05 and 0.1 wt.% mixed metal (Ce, La) was better than that of undoped alloy due to the decrease of surface tension [21]. The results imply that both the addition of Zn and rare earth elements into solders is advantageous for the physical and mechanical properties, without the concern of rapid whisker growth. In addition, the optimized alloying contents are of interest.

In this study, 0.5 wt.% Ce accompanied by 0.2 wt.% and 0.5 wt.% Zn were added into the Sn–3Ag–0.5Cu solders. The whisker growth and the properties of Sn–3Ag–0.5Cu–0.5Ce–*x*Zn alloys, namely the microstructure, mechanical properties, melting behavior and intermetallic reactions in BGA packages with Au/Ni surface finishes, were evaluated.

2. Experimental

The Sn–3Ag–0.5Cu–0.5Ce, Sn–3Ag–0.5Cu–0.5Ce–0.2Zn and Sn–3Ag–0.5Cu–0.5Ce–0.5Zn alloys used in this study were prepared by induction melting of a Sn–6.6 wt.% Ce master alloy at 1000 °C under 10^{-5} Pa vacuum and then remelting it with the addition of the elements Sn, Ag, Cu and Zn in a quartz ampoule under the same conditions. For comparison, undoped Sn–3Ag–0.5Cu solder was also melted and cast in vacuum. These ampoules were then water quenched, with a cooling rate of about 300 °C/s. After solidification, the ingots were cold rolled into 0.18 mm thick plates from which tensile test specimens, as shown in Fig. 1, were punched. Tensile-tested using an MTS-Tytron 250 Microforce tester at a crosshead speed of 0.01 mm/s. The average values of every tensile strength and elongation were estimated from at least 5 measurements. In addition, differential scanning calorimetry (DSC) was used to determine the melting temperatures of solder alloys. The heating rate for the DSC test was 5 °C/min in nitrogen atmosphere. Some of the solder plates were further punched into disks of 0.45 mm in diameter.

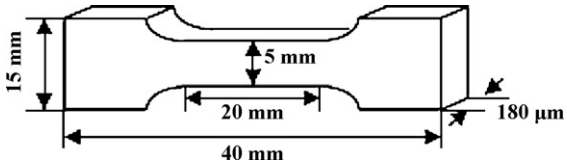

Fig. 1. Dimensions of Sn–3Ag–0.5Cu–0.5Ce–*x*Zn alloys for tensile tests.

Table 1
Melting temperatures and mechanical properties of Sn–3Ag–0.5Cu and Sn–3Ag–0.5Cu–0.5Ce–*x*Zn solders.

Solder alloys	Eutectic point (°C)	Tensile strength (MPa)	Elongation (%)
Sn–3Ag–0.5Cu	217.5	43.7	29.6
Sn–3Ag–0.5Cu–0.5Ce	218.7	21.9	15.9
Sn–3Ag–0.5Cu–0.5Ce–0.2Zn	219.1	65.3	17.1
Sn–3Ag–0.5Cu–0.5Ce–0.5Zn	217.8	64.3	18.9

The solder disks, after being dipped in rosin mildly activated flux, were placed on the Electroless Ni(2.54 μm thick)/Immersion Au(75 nm thick) surface finished Cu pads of ball grid array(BGA) packages. The specimens were then reflowed in a hot-air furnace using a temperature profile with the soaking temperature and peak temperature at 190 °C and 240 °C, respectively. The surface tension of the molten solder caused the solder disks to become solder balls after solidification. After reflow, aging treatments were performed at 100 °C and 150 °C for various times, ranging from 100 to 1000 h. The reflowed and aged specimens were cut from cross-sections of a row of solder balls, ground with 2000 grit SiC paper, and polished with 0.3 μm Al_2O_3 powder. The IMCs were observed via scanning electron microscopy (SEM), and their chemical compositions were analysed using an energy-dispersive X-ray spectroscope (EDX) installed in the SEM.

The bonding strengths of the solder balls on the Au/Ni/Cu pads under reflow and various aging conditions were measured via ball shear tests. For this purpose, the ball shear rate was fixed at 0.1 mm/s with a shear height of 80 μm (about 1/4 the reflowed ball height). After the ball shear tests, the fractography of the fractured solder joints was observed with SEM.

3. Results and discussion

The microstructures of the as cast Sn–3Ag–0.5Cu (SAC305), Sn–3Ag–0.5Cu–0.5Ce (SAC305Ce), Sn–3Ag–0.5Cu–0.5Ce–0.2Zn

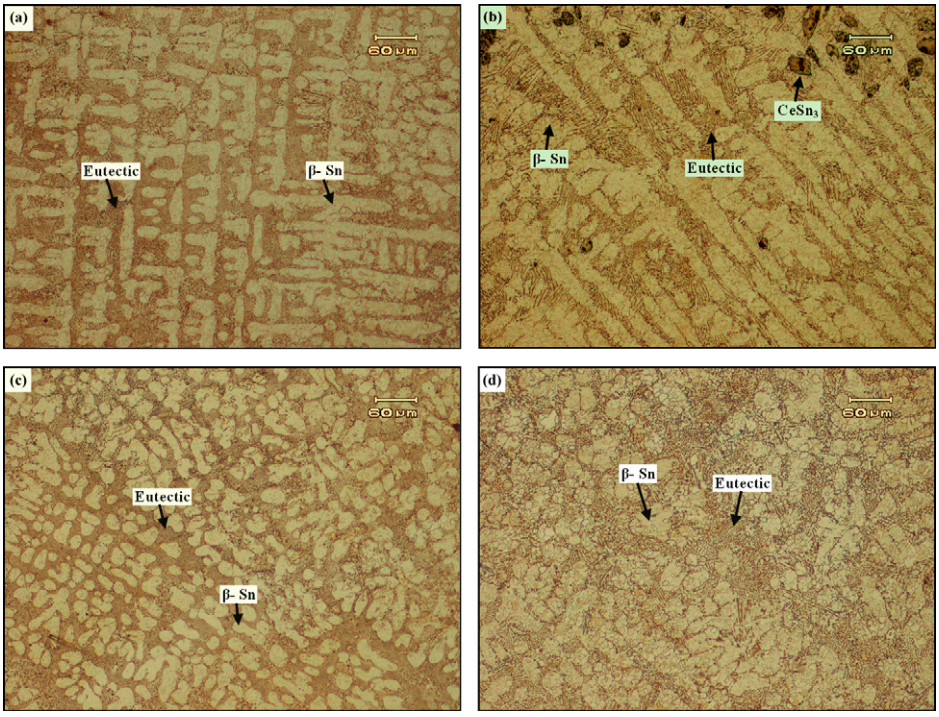

Fig. 2. Optical micrographs for: (a) Sn–3Ag–0.5Cu; (b) Sn–3Ag–0.5Cu–0.5Ce; (c) Sn–3Ag–0.5Cu–0.5Ce–0.2Zn; and (d) Sn–3Ag–0.5Cu–0.5Ce–0.5Zn.

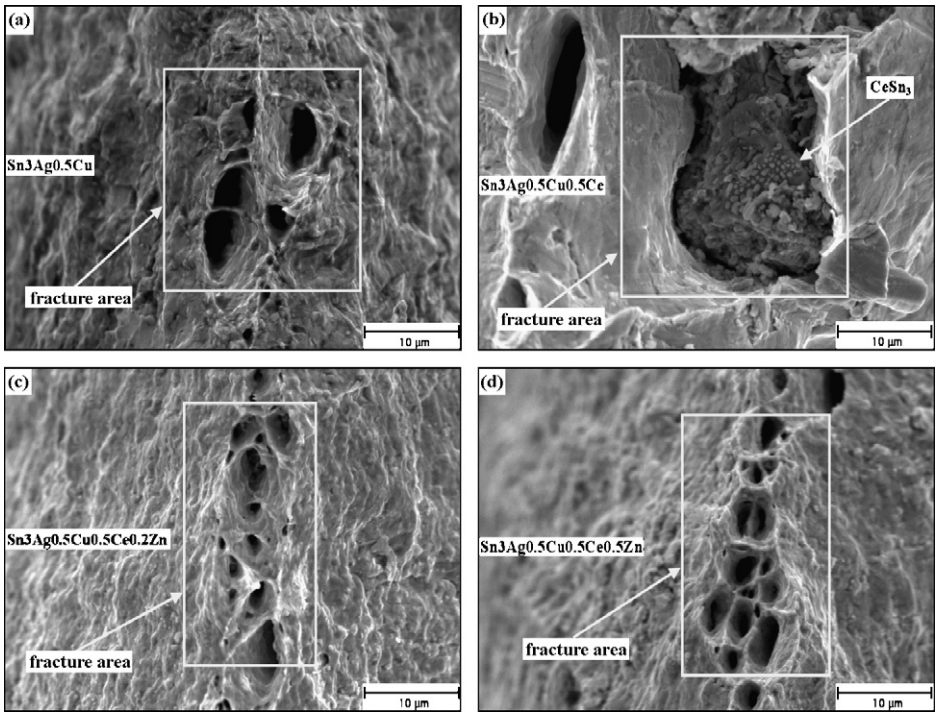

Fig. 3. The fractographs after tensile tests for: (a) Sn–3Ag–0.5Cu; (b) Sn–3Ag–0.5Cu–0.5Ce; (c) Sn–3Ag–0.5Cu–0.5Ce–0.2Zn; and (d) Sn–3Ag–0.5Cu–0.5Ce–0.5Zn.

(SAC305Ce0.2Zn) and Sn–3Ag–0.5Cu–0.5Ce–0.5Zn (SAC305Ce0.5Zn) alloys are shown in Fig. 2. They consist of the light-colored coarse β-Sn phase surrounded by dark eutectic networks of β-Sn, Cu_6Sn_5 and Ag_3Sn phases. For the Zn-undoped SAC305 and SAC305Ce solders, the coarse β-Sn phase appears as a dendritic structure. Fig. 2b also shows many large RE-containing $CeSn_3$ intermetallic clusters in the solder matrix. With the further addition of 0.2 and 0.5 wt.% Zn into the SAC305Ce solder, the dendrite structures of β-Sn phase break into granular shapes and the $CeSn_3$ intermetallic clusters disappear, as shown in Fig. 2c and d. Our previous study [16] provided evidence that the doping with Zn into the Sn–3Ag–0.5Cu–0.5Ce alloy can cause the large $CeSn_3$ clusters to become very fine (Ce, Zn)Sn_3 particles.

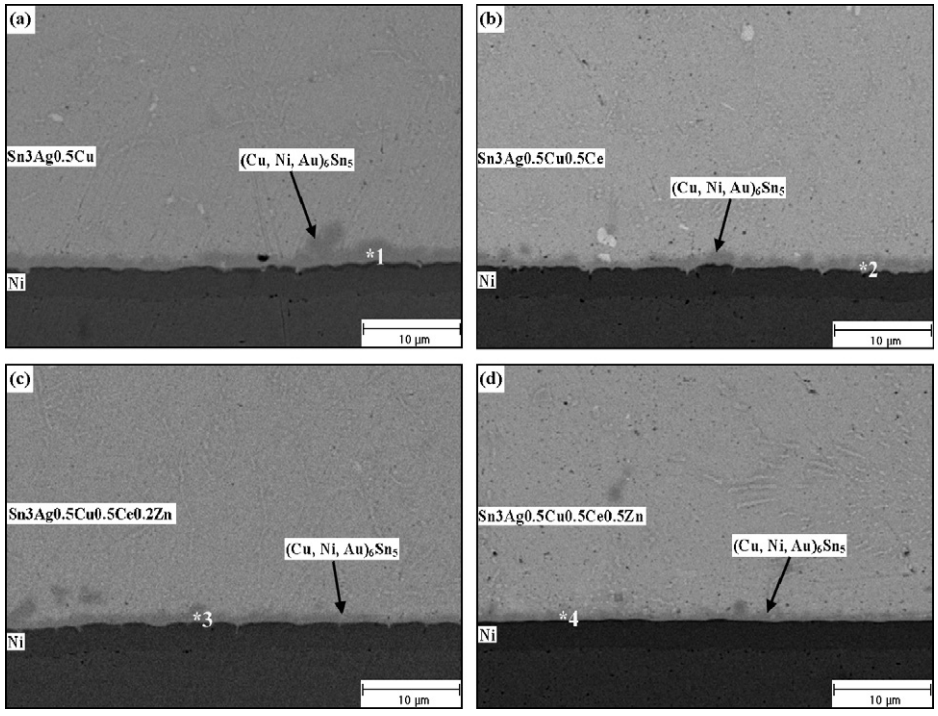

Fig. 4. Morphology of intermetallic compounds formed in Sn–3Ag–0.5Cu–0.5Ce–*x*Zn solder BGA packages with Au/Ni/Cu pads after reflow: (a) Sn–3Ag–0.5Cu; (b) Sn–3Ag–0.5Cu–0.5Ce; (c) Sn–3Ag–0.5Cu–0.5Ce–0.2Zn; and (d) Sn–3Ag–0.5Cu–0.5Ce–0.5Zn.

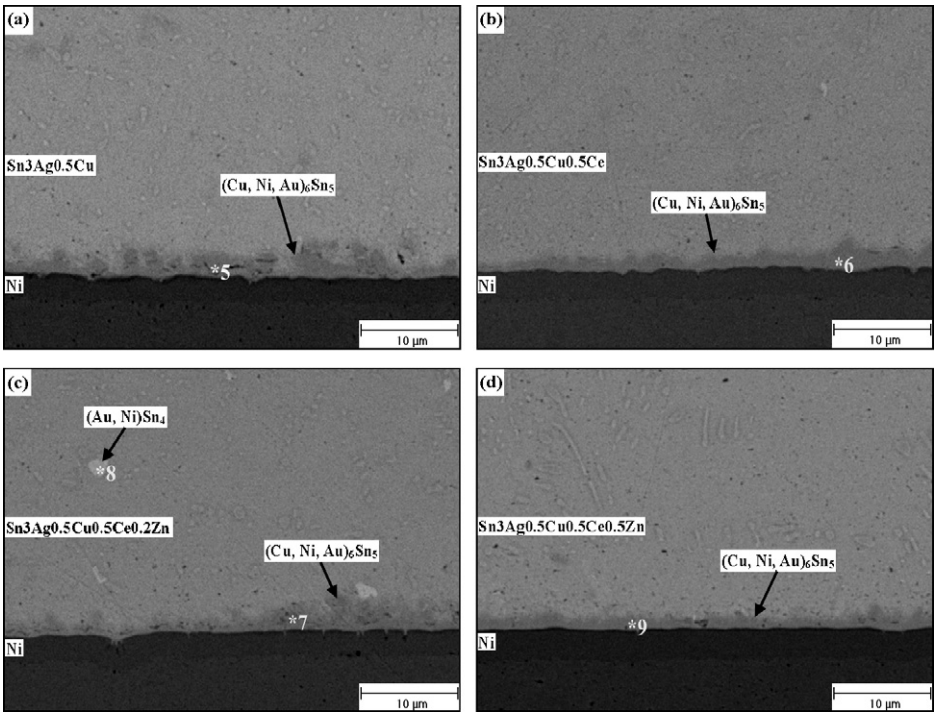

Fig. 5. Morphology of intermetallic compounds formed in Sn–3Ag–0.5Cu–0.5Ce–*x*Zn solder BGA packages with Au/Ni/Cu pads after aging at 100 °C for 1000 h: (a) Sn–3Ag–0.5Cu; (b) Sn–3Ag–0.5Cu–0.5Ce; (c) Sn–3Ag–0.5Cu–0.5Ce–0.2Zn; and (d) Sn–3Ag–0.5Cu–0.5Ce–0.5Zn.

It has been reported that the doping with rare earth elements can reduce the melting temperature of solder alloys [22]. However, such an advantageous effect was not found in this study. DSC analyses indicate that the eutectic points, which are listed in Table 1 for various Sn–Ag–Cu solders, increased slightly in the sequence of SAC305 < SAC305Ce < SAC305Ce0.2Zn. Table 1 also demonstrates the ultimate tensile strength and elongation of various alloys in this study. In comparison to the undoped SAC305 solder, the tensile strength of SAC305Ce decreased drastically from 43.7 to 21.9 MPa due to the addition of 0.5 wt.% Ce. Accompanying the large decay of tensile strength for SAC305 solder doped with 0.5 wt.% Ce, its elongation also dropped from 29.6% to 15.9%. The coarse $CeSn_3$ phase in this high RE-containing solder can cause severe embrittlement and poor mechanical properties for the solder alloy.

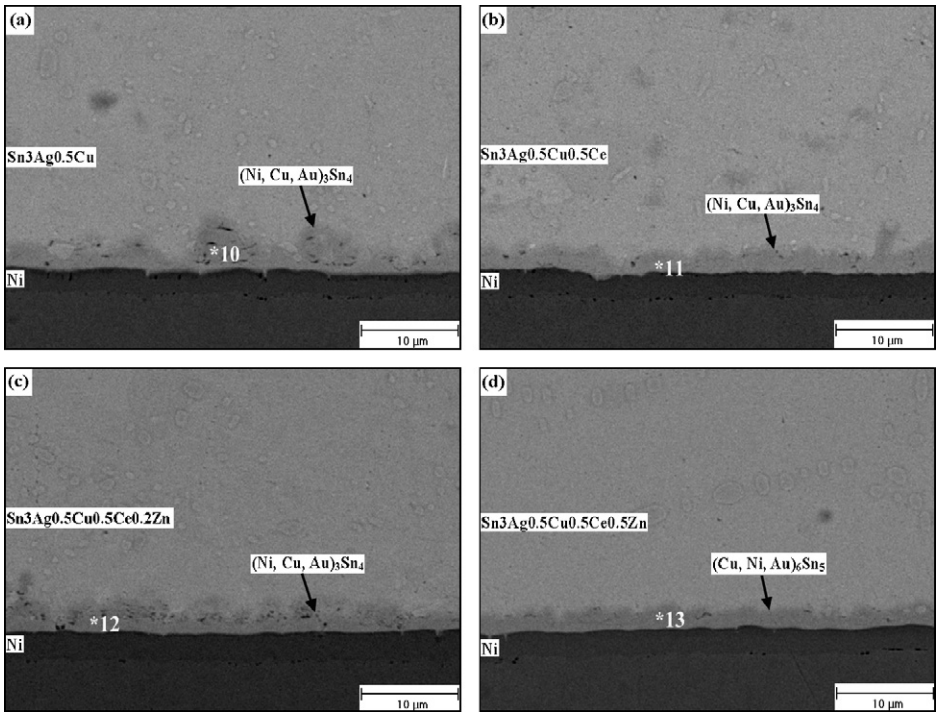

Fig. 6. Morphology of intermetallic compounds formed in Sn–3Ag–0.5Cu–0.5Ce–*x*Zn solder BGA packages with Au/Ni/Cu pads after aging at 150 °C for 1000 h: (a) Sn–3Ag–0.5Cu; (b) Sn–3Ag–0.5Cu–0.5Ce; (c) Sn–3Ag–0.5Cu–0.5Ce–0.2Zn; and (d) Sn–3Ag–0.5Cu–0.5Ce–0.5Zn.

Table 2
Chemical compositions of intermetallic compounds formed in Sn–3Ag–0.5Cu–0.5Ce–*x*Zn solder BGA packages with Au/Ni/Cu pads after reflow and different aging treatments.

Reference points	Phase	Compositions (at.%)			
		Sn	Cu	Au	Ni
1	$(Cu, Ni, Au)_6Sn_5$	42.7	33.6	0.6	23.1
2	$(Cu, Ni, Au)_6Sn_5$	43.4	34.2	0.5	21.9
3	$(Cu, Ni, Au)_6Sn_5$	43.2	33.1	0.5	23.2
4	$(Cu, Ni, Au)_6Sn_5$	43.1	34.2	1.1	21.6
5	$(Cu, Ni, Au)_6Sn_5$	43.1	40.1	0.4	16.4
6	$(Cu, Ni, Au)_6Sn_5$	43.4	36.2	0.8	19.6
7	$(Cu, Ni, Au)_6Sn_5$	43.4	40.4	0.7	15.5
8	$(Au, Ni)Sn_4$	80.2	–	11.6	8.2
9	$(Cu, Ni, Au)_6Sn_5$	43.3	33.2	0.7	22.8
10	$(Ni, Cu, Au)_3Sn_4$	52.4	11.4	0.3	35.9
11	$(Ni, Cu, Au)_3Sn_4$	51.1	10.2	0.3	38.4
12	$(Ni, Cu, Au)_3Sn_4$	53.7	8.6	0.6	37.1
13	$(Cu, Ni, Au)_6Sn_5$	46.3	27.1	0.9	25.7

It is interesting that the degradation of tensile strength of SAC305Ce solder can be significantly improved through further addition of Zn element. Table 1 reveals that the tensile strength of SAC305Ce solder has been drastically increased from 21.9 to 65.3 and 64.3 MPa by the alloying with 0.2 and 0.5 wt.% Zn, respectively. The tensile strengths of both Zn-doped SAC305Ce solders are even higher than that of original Sn–3Ag–0.5Cu alloy (43.7 MPa). Although the ductility of SAC305Ce has also been improved through further Zn-doping, as shown in Table 1, the elongations of both SAC305Ce0.2Zn and SAC305Ce0.5Zn solders are still much lower than those of the Ce and Zn-free SAC305 solder.

Fractography of all bulk solders after tensile tests revealed dimple characteristics, as shown in Fig. 3. In certain cases, RE-containing intermetallics were embedded in the dimples, as shown in Fig. 3b. The result indicates that dislocations accumulated at the intermetallics/matrix interface during the tensile testing, which induced stress concentration to rupture the specimens predominately through these regions. The degradation of the tensile strength of SAC305Ce alloy is ascribed to the severer stress concentration caused by the coarser $CeSn_3$ intermetallics in SAC305Ce solder matrix. On the other hand, the finer and more uniformly distributed $(Ce, Zn)Sn_3$ intermetallics in Zn-doped SAC305Ce alloys cannot only obstruct the movement of dislocations but also cause less stress concentration, which combine to lead higher tensile strengths than the Zn-free solder. However, such a strengthening effect would also sacrifice a certain amount of ductility in the solder matrix. Comparing the results in Table 1, it appears that the fine $(Ce, Zn)Sn_3$ intermetallic particles in both Zn-doped SAC305Ce alloys lead to higher elongations than that of the Zn-free SAC305Ce with coarse $CeSn_3$, while they cannot recover the ductility of Ce- and Zn-free Sn–3Ag–0.5Cu solder.

Fig. 4 shows the microstructure of reflowed solder joints for various Sn–Ag–Cu solder packages with Au/Ni/Cu pads in this study. The chemical compositions of the reference points shown in Figs. 4–6 are listed in Table 2. The chemical compositions (at.%) of intermetallic layers formed at all reflowed solder/pad interfaces were similar to Cu:Ni:Au:Sn = 33.6:23.1:0.6:42.7, which corresponds to a $(Cu, Ni, Au)_6Sn_5$ phase. The Ce and Zn contents cannot be detected in these interfacial intermetallics of solder joints. It can be seen in Fig. 4 that the thickness of intermetallics compounds at the solder/pad interface of SAC305 packages (Fig. 4a) is obviously thicker than those in the other Sn–Ag–Cu solder joints doped with 0.5 wt.% Ce. The depressing effect of interfacial intermetallics in the Ce-containing SAC305 solder joints is attributed to their shorter solidification time due to the more heterogeneous nucleation sites providing by $CeSn_3$ phases in the solder matrix.

After aging at 100 °C for 1000 h, the intermetallic compounds formed at all solder/Ni interfaces remained as $(Cu, Ni, Au)_6Sn_5$, as shown in Fig. 5. The growth rate of $(Cu, Ni, Au)_6Sn_5$ in SAC305Ce0.5Zn solder joints with Au/Ni/Cu pads was lowest among all solder joints. The activity of Sn atoms at the inter-

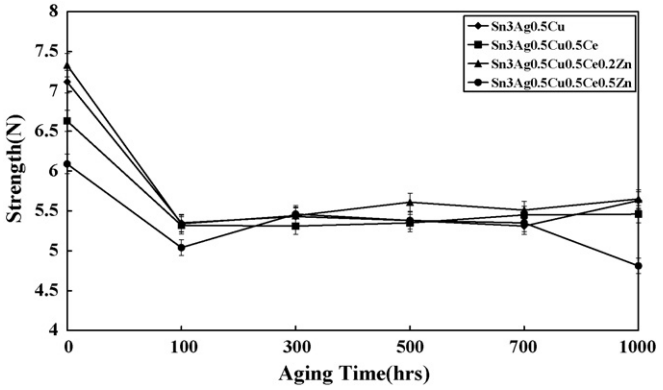

Fig. 7. Ball shear strengths of various Sn–Ag–Cu solder BGA packages with Au/Ni/Cu pads after aging at 100 °C for various times.

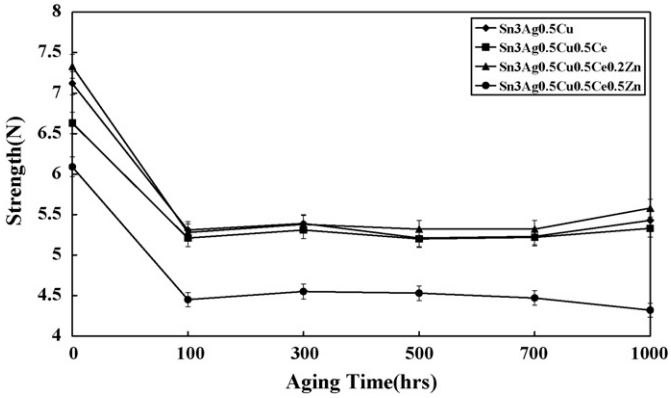

Fig. 8. Ball shear strengths of various Sn–Ag–Cu solder BGA packages with Au/Ni/Cu pads after aging at 150 °C for various times.

Table 3
Ball shear strengths of the Sn–3Ag–0.5Cu and Sn–3Ag–0.5Cu–0.5Ce–*x*Zn solder BGA packages with Au/Ni/Cu pads after various aging treatments.

Surface finishing:	Au/Ni/Cu pads							
Solder joints:	Sn–3Ag–0.5Cu		Sn–3Ag–0.5Cu–0.5Ce		Sn–3Ag–0.5Cu–0.5Ce–0.2Zn		Sn–3Ag–0.5Cu–0.5Ce–0.5Zn	
Aging:	100 °C	150 °C	100 °C	150 °C	100 °C	150 °C	100 °C	150 °C
0	7.1 N	7.1 N	6.6 N	6.6 N	7.3 N	7.3 N	6.1 N	6.1 N
100 h	5.4 N	5.3 N	5.3 N	5.2 N	5.3 N	5.3 N	5.0 N	4.5 N
300 h	5.4 N	5.4 N	5.3 N	5.3 N	5.4 N	5.4 N	5.5 N	4.6 N
500 h	5.4 N	5.2 N	5.4 N	5.2 N	5.6 N	5.3 N	5.4 N	4.5 N
700 h	5.3 N	5.2 N	5.5 N	5.2 N	5.5 N	5.3 N	5.4 N	4.5 N
1000 h	5.6 N	5.4 N	5.5 N	5.3 N	5.7 N	5.6 N	4.8 N	4.3 N

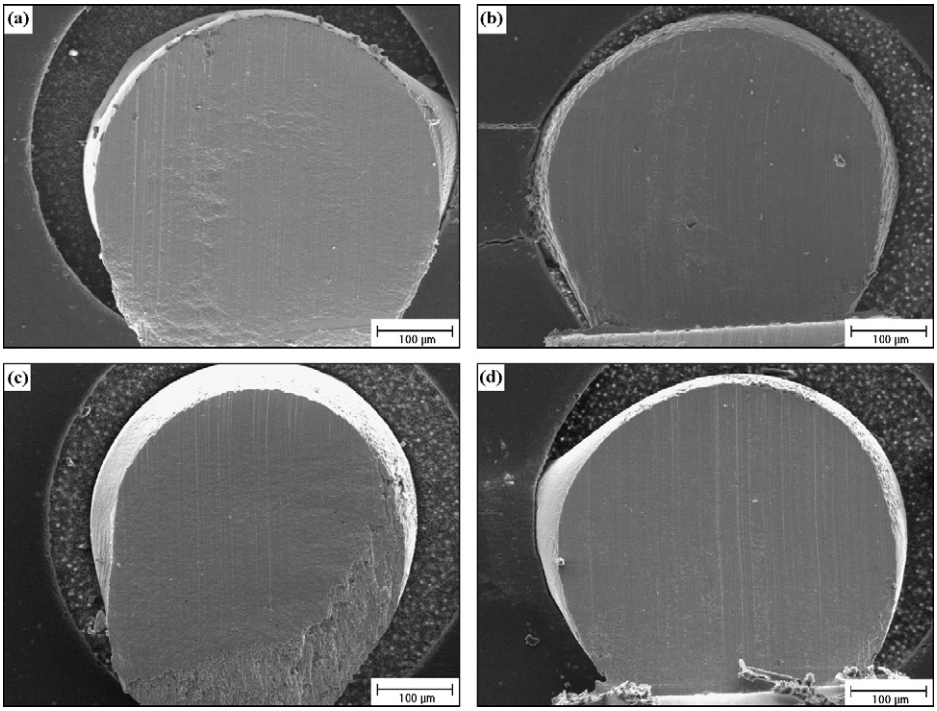

Fig. 9. Typical fractography of as reflowed solder joints after ball shear tests: (a) Sn–3Ag–0.5Cu, (b) Sn–3Ag–0.5Cu–0.5Ce, (c) Sn–3Ag–0.5Cu–0.5Ce–0.2Zn, and (d) Sn–3Ag–0.5Cu–0.5Ce–0.5Zn.

face of the (Cu, Ni, Au)$_6$Sn$_5$ IMC/solder was lowered as a result of the formation of Ce-containing intermetallic compounds, which can hamper the diffusion of Sn atoms. Since there are more uniformly distributed and finer rare earth containing intermetallics in SAC305Ce0.5Zn solder joints, the inhibition effect on the (Cu, Ni, Au)$_6$Sn$_5$ growth is more obvious than in the other solder joints. Fig. 6 indicates that the intermetallic compounds formed at SAC305, SAC305Ce and SAC305Ce0.2Zn solder/Ni interface were transformed from (Cu, Ni, Au)$_6$Sn$_5$ to (Ni, Cu, Au)$_3$Sn$_4$ after aging at 150 °C for 1000 h. With the increase in aging time and aging temperature, Ni atoms would have sufficient energy and time to diffuse, and the (Cu, Ni, Au)$_6$Sn$_5$ compounds formed at solder/Ni interface were transformed to (Ni, Cu, Au)$_3$Sn$_4$ due to the lower standard Gibbs energies of formation of (Ni, Cu, Au)$_3$Sn$_4$ than (Cu,

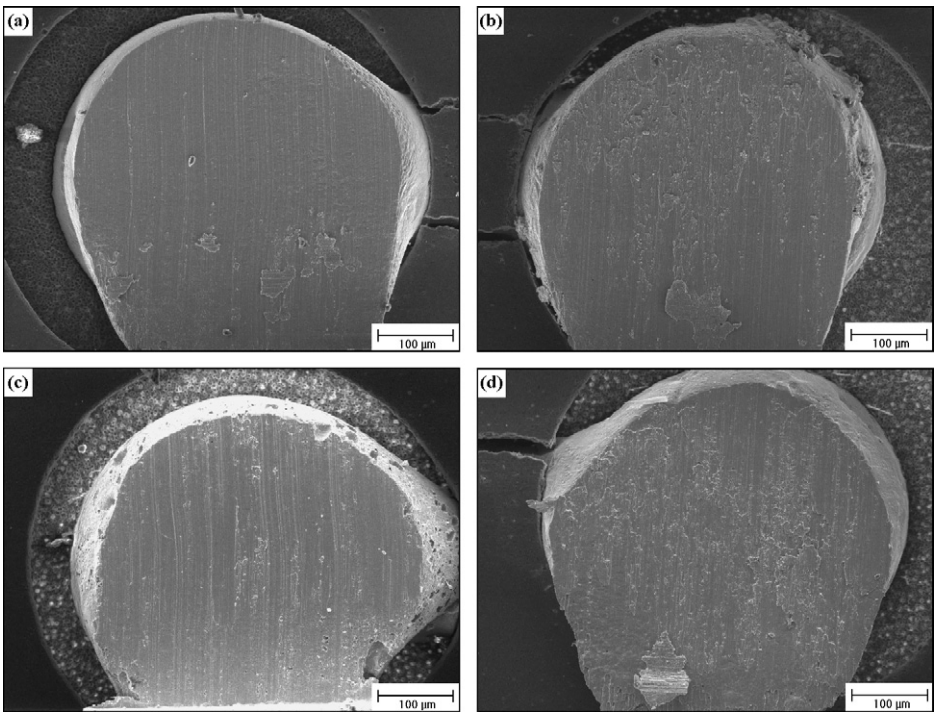

Fig. 10. Typical fractography of 150 °C, 1000 h aged solder joints after ball shear tests: (a) Sn–3Ag–0.5Cu, (b) Sn–3Ag–0.5Cu–0.5Ce, (c) Sn–3Ag–0.5Cu–0.5Ce–0.2Zn, and (d) Sn–3Ag–0.5Cu–0.5Ce–0.5Zn.

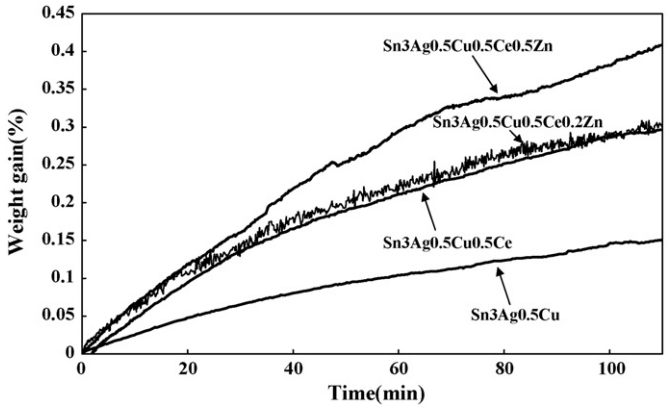

Fig. 11. Weight gain percentages of Sn–3Ag–0.5Cu, Sn–3Ag–0.5Cu–0.5Ce, Sn–3Ag–0.5Cu–0.5Ce–0.2Zn and Sn–3Ag–0.5Cu–0.5Ce–0.5Zn alloys during 150 °C oxidation reactions in air.

Ni, Au)$_6$Sn$_5$. The time required for the transformation of (Cu, Ni, Au)$_6$Sn$_5$ in SAC305Ce0.5Zn solder joints is longer than that of the other solder joints, since Ni and Zn have a stronger affinity than Ni and Sn and thus the interaction between Sn and Ni would be seriously weakened due to the existence of Zn. The time required for the transformation of (Cu, Ni, Au)$_6$Sn$_5$ was increased with more Zn added. Figs. 7 and 8 provide the results of ball shear tests for various Sn–Ag–Cu solder BGA packages after reflow and aging processes, respectively. The bonding strengths are listed in Table 3. Fractography of all reflowed and aged specimens after ball shear tests reveal ductile characteristics across the solder balls, as shown in Figs. 9 and 10, respectively. The SAC305Ce0.5Zn solder BGA package possesses the lowest ball shear strength among these reflowed solder joints. Since the soldering reaction during the reflowing process would be obstructed by the oxide, the worst bonding strength, that in the SAC305Ce0.5Zn solder joint, might be related to its poorest oxidation resistance. This suspicion is strengthened by Fig. 11, which shows that the TGA curve of the weight gain percentage for the SAC305Ce0.5Zn specimen during air storage at 150 °C is much higher than those for the SAC305, SAC305Ce and SAC305Ce0.2Zn specimens. The oxidation rate of Sn–3Ag–0.5Cu solder alloy increased with more Ce and Zn additions because Ce and Zn atoms are highly chemically active. Aging treatments resulted in the softening of the solder matrix, which led to the degradation of ball shear strengths in all BGA packages. Finally, the inhibition of tin whiskers has been confirmed in Fig. 12 that the addition of 0.2 wt.% Zn into the Sn–3Ag–0.5Cu–0.5Ce solder is sufficient to prevent the formation of fiber shaped whiskers and coarse hillocks after prolonged air exposure at room temperature and 150 °C, respectively, which were observed previously in Ce-containing SAC305 solders without Zn-doping [12,13].

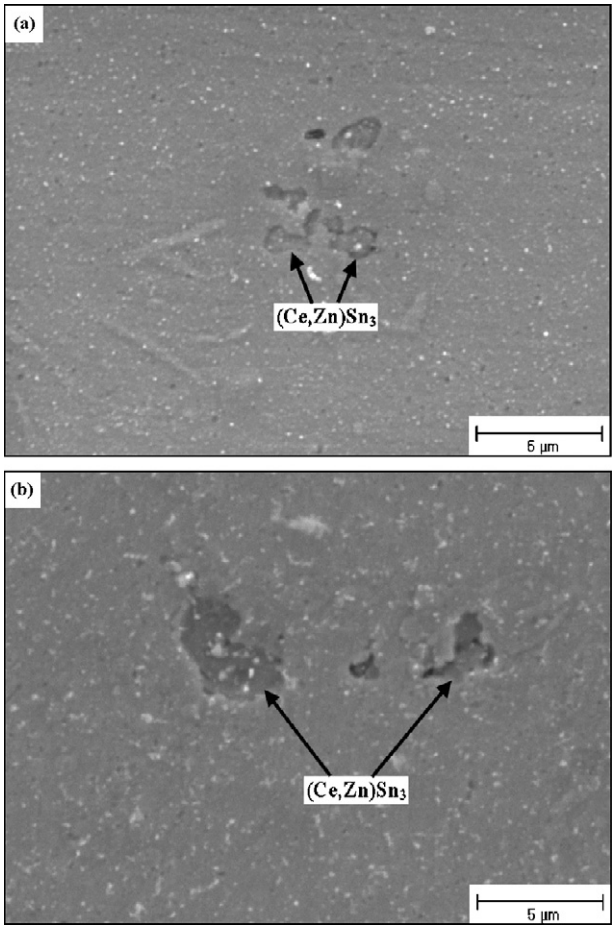

Fig. 12. Microstructure of the (Ce, Zn)Sn_3 intermetallics on the surface of Sn–3Ag–0.5Cu–0.5Ce–0.2Zn solders after air exposure at (a) room temperature and (b) 150 °C for 21 days.

4. Conclusions

The coarse $CeSn_3$ intermetallic clusters in Sn–3Ag–0.5Cu–0.5Ce alloy not only cause the rapid growth of tin whiskers but also severely degrade its tensile strength and ductility. With 0.2 or 0.5 wt.% Zn addition into this Ce-containing Sn–Ag–Cu solder, the tensile strengths are significantly improved and the phenomenon of rapid whisker growth is prevented. The elongations of both Zn containing bulk solders are higher than that of the Sn–3Ag–0.5Cu–0.5Ce, although they are still lower than that of the original Sn–3Ag–0.5Cu. The intermetallic compounds formed at the solder/pad interfaces were depressed in such Zn-doped Sn–3Ag–0.5Cu–0.5Ce solder packages. However, excess Zn addition to 0.5 wt.% causes the decrease of ball shear strength after reflowing and aging processes due to higher oxidation rate. The optimized Sn–3Ag–0.5Cu–0.5Ce–0.2Zn alloy possesses the highest bonding strength among the Sn–Ag–Cu solder joints in this study, and is free of the problem of rapid whisker growth.

Acknowledgements

This work was sponsored by the National Science Council, Taiwan, under grant number NSC-96-2221-E002-150-MY3. The support from National Taiwan University and Industrial Technology Research Institute, Taiwan, is also greatly appreciated.

References

[1] K. Zeng, K.N. Tu, Mater. Sci. Eng. R 38 (2002) 55–105.
[2] J. Zhou, D. Huang, Y.L. Fang, F. Xue, J. Alloys Compd. 480 (2009) 903–907.
[3] G.D. Li, Y.W. Shi, H. Hao, Z.D. Xia, Y.P. Lei, X.Y. Li, J. Mater. Sci.: Mater. Electron 20 (2009) 186–192.
[4] D.Q. Yu, J. Zhao, L. Wang, J. Alloys Compd. 376 (2004) 170–175.
[5] R. Mahmudi, A.R. Geranmayeh, B. Zahiri, M.H. Marvasti, J. Mater. Sci.: Mater. Electron 21 (2010) 58–64.
[6] J.X. Wang, S.B. Xue, Z.J. Han, S.L. Yu, Y. Chen, Y.P. Shi, H. Wang, J. Alloys Compd. 467 (2009) 219–226.
[7] Y.Y. Shiue, T.H. Chuang, J. Alloys Compd. 491 (2010) 610–617.
[8] W.M. Xiao, Y.W. Shi, G.C. Xu, R. Ren, F. Guo, Z.D. Xia, Y.P. Lei, J. Alloys Compd. 472 (2009) 198–202.
[9] Y.W. Shi, J. Tian, H. Hao, Z.D. Xia, Y.P. Lei, F. Guo, J. Alloys Compd. 453 (2008) 180–184.
[10] M.A. Dudek, R.S. Sidhu, N. Chawla, M. Renavikar, J. Electron. Mater. 35 (2006) 2088–2097.
[11] M.A. Dudek, N. Chawla, Metall. Mater. Trans. 41A (2010) 610–620.
[12] T.H. Chuang, S.F. Yen, J. Electron. Mater. 35 (2006) 1621–1627.
[13] T.H. Chuang, Metall. Mater. Trans. 38A (2007) 1048–1055.

[14] T.H. Chuang, H.J. Lin, Metall. Mater. Trans. 39A (2008) 2862–2866.
[15] H.J. Lin, T.H. Chuang, J. Electron. Mater. 39 (2010) 200–208.
[16] T.H. Chuang, H.J. Lin, J. Electron. Mater. 38 (2009) 420–424.
[17] F.J. Wang, X. Ma, Y.Y. Qian, Scr. Mater. 53 (2005) 699–702.
[18] S.K. Kang, D.J. Shih, D. Leonard, D.W. Henderson, T. Gosselin, S. Cho, J. Yu, W.K. Choi, JOM 56 (2004) 34–38.
[19] F.J. Wang, F. Gao, X. Ma, Y.Y. Qian, J. Electron. Mater. 35 (2006) 1818–1824.
[20] C.M.L. Wu, D.Q. Yu, C.M.T. Law, L. Wang, J. Electron. Mater. 31 (2002) 921–927.
[21] C.M.L. Wu, C.M.T. Law, D.Q. Yu, L. Wang, J. Electron. Mater. 32 (2002) 63–69.
[22] C.M.L. Wu, D.Q. Yu, C.M.T. Law, L. Wang, Mater. Sci. Eng. R 44 (2004) 1–44.